https://doi.org/10.5194/egusphere-2024-1276
Preprint. Discussion started: 30 May 2024

Investigation of Different Roughness Approaches and Vegetation Height Effects on rain-induced overland flow

Azam Masoodi[1], Philipp Kraft[1]
[1]Department of Landscape Ecology and Resources Management, Justus Liebig University Giessen, 35392, Germany
Correspondence to: Azam Masoodi (Azam.Masoodi@umwelt.uni-giessen.de)

Abstract. Overland flow is a critical aspect of the hydrological cycle, and understanding its dynamics is crucial for managing water-related issues such as flooding and soil erosion. This paper investigates the impact of various roughness estimation methods on simulating overland flow during intense rain events, with a specific focus on the influence of vegetation. The study assesses various approaches to vary roughness as a function of water sheet thickness and vegetation height, including two different constant Manning's coefficients, a linear approach, an exponential function, a power law function, an empirical formula, and a physics-based approach. The investigation emphasizes the importance of accurate roughness estimation for improving the reliability of hydrological models and enhancing flood prediction capabilities. Experimental data from artificial rainfall experiments on 22 different natural hillslopes in Germany are used to calibrate the OpenLISEM hydrological model, adjusting parameters such as saturated hydraulic conductivity and soil suction at the wetting front. Subsequently, various Manning's coefficient estimation methods are applied, and the model's performance is evaluated numerically.
Preliminary results indicate satisfactory calibration outcomes, with NSE values ranging from 0.75 to 0.95 in most cases for various sites. To validate the models, 100 different experimental rainfall events are used for each roughness method. Validation findings suggest that the physics-based approach, the linear function, and constant Manning roughness, demonstrate the best performance based on NSE values. According to our results, areas with more vegetation coverage demonstrate higher saturated hydraulic conductivity value, indicating that, for two sites with the same soil type, the locations with dense vegetation exhibit higher infiltration parameters. Consequently, it is crucial to evaluate the influence of vegetation on runoff, considering not only its effects on Manning's coefficient but also on saturated hydraulic conductivity.

1 Introduction

Catchment vegetation plays a key role in the hydrological cycle (Peel, 2009). Flow-vegetation interactions effect on the runoff by increasing the roughness, modifying flow patterns, and providing additional drag (Vargas-Luna et al., 2015). Numerous field, experimental and analytical studies have been conducted to explore the effects of submerged or emergent vegetation on runoff (Aberle and Järvelä, 2015; Freeman et al., 2000; Nepf, 2012; Nicosia and Ferro, 2023). The velocity profile is typically consistent throughout the depth in cases of emergent vegetation, whereas for submerged vegetation, the velocity profile exhibits an approximately S-shaped pattern. This results in a Kelvin-Helmholtz instability between the upper flow and the flow between the vegetation (D'Ippolito et al., 2021). Nepf, (2012) stated that the flow behavior of the submerged grassland can be categorized into two limits, based on the relative significance of bed shear and grassland drag. Based on Järvelä's study the primary factors influencing the Darcy-Weisbach friction factor were relative roughness, flow velocity, and flow depth (Järvelä, 2002). The significance of these factors varied based on whether the flow was submerged or not. Additionally, Järvelä introduced an approach to assess the Darcy-Weisbach friction factor caused by rigid and flexible woody vegetation in situations non-submerged flow (Järvelä, 2004). Oberle et al. (2021) investigated flow depth-dependent roughness relationships using some experimental data on homogeneous artificial grass (Ruiz Rodriguez, 2017). They found roughness coefficient values varied with different water depths. Hinsberger et al. (2022) conducted laboratory experiments involving both submerged and emergent vegetation, along with solid surfaces. Determined roughness coefficients were then used to assess how water depth and slope impact roughness. In the case of submerged vegetation, changes in water depth demonstrated a reduction in roughness as submergence increased. Conversely, for emergent vegetation, greater submergence resulted in heightened

https://doi.org/10.5194/egusphere-2024-1276
Preprint. Discussion started: 30 May 2024

roughness. These results are in agreement with Oberle et al. (2021). Their findings demonstrated that the relationship between roughness and water depth for the intermediate area can be effectively characterized using a linear method. A Review of recent studies indicates that a variety of surface roughness equations have been developed to formulate the relevant roughness caused by vegetation (D'Ippolito et al., 2021). The uncertainty of resistance coefficient values leads to varying results in surface runoff accumulation. Dalledonne et al., (2019) introduced an approach to evaluate uncertainty in floodplain hydrodynamic models influenced by vegetation, testing four resistance formulas. Meanwhile, Kiczko et al., (2020) compared advanced process-based methods with practical divided channel techniques for estimating discharge in vegetated river channels. Their findings indicated the superiority of complex process-based methods over the Manning-based divided channel method, consistent with Dalledonne et al., (2019)'s observations of narrower uncertainty estimates associated with complex models. Feldmann et al. (2023) proposed a framework to estimate Manning roughness dependent on shallow water depth. First, the partitioning of runoff and infiltration was calculated during the descending limb of the hydrograph to determine the minimum infiltration rate. Then, they reduced the solution space by comparing experiments conducted at one site and by comparing sites with similar properties. The framework's robustness was tested using three different depth-dependent roughness equations and a constant Manning coefficient using artificial rainfall experiments conducted by Ries et al. (2020).

Utilizing flow resistance models in vegetated areas holds immense value in evaluating the potential for flooding and formulating flood mitigation strategies grounded in scientific principles (Green, 2005). However, evaluating these equations to calculate overland flows continues to be a staple area of research within hydrology. To test the effect different roughness calculation methods, they need to be included into a complete surface runoff model. OpenLISEM (Open LImburg Soil Erosion Model) was chosen for its modular structure, open source code and physics-based approach. It allows to see, modify, and distribute the code by users. It is an event-based and spatial hydrological model suitable for different sizes of catchments. It focuses on simulating runoff, sediment dynamics, and infiltration during heavy rainstorms, allowing for detailed assessments of land use changes and conservation measures (Jetten, 2002). With the development of OpenLISEM by roughness estimation models, it is possible to calculate the effects of flow through or over the vegetation.

To develop and evaluate runoff models in the absence of real measurement, artificial sprinkling studies present an opportunity to investigate roughness coefficients. Ries et al. (2020) collected one of the most extensive datasets accessible in southwest Germany. By utilizing the experimental dataset from Ries et al. (2020) and hydrodynamic simulation, our study takes a significant step forward in assessing the accuracy of roughness coefficient estimations. This assessment covers a variety of scenarios involving different levels of vegetation coverage and vegetation height and varying rainfall intensities.

The scope of our study encompasses the following objectives:

- Investigation of vegetation effects on overland flow
- Modelling the overland flow to compare and validation of different approaches of Manning's coefficient estimation
- Investigation of initial and boundary condition effects on modeling

By comparing observed and simulated discharge, we evaluate the effectiveness of different approaches to estimate Manning's coefficient. Furthermore, our study provides clear insights into initial condition effects on overland flow hydrodynamics and the relationship between vegetation and runoff depth.

2 Materials and methods

2.1 Model

To explore the impact of roughness on overland flow simulations, it's crucial to integrate the relationship between roughness and water depth into the model. For this purpose, OpenLISEM version 6.873 has been utilized which employs Manning's approach to calculate the runoff velocity. While the original software employed a constant Manning's coefficient as a raster map for roughness, a new feature called the dynamic Manning's n function has been introduced into the software to implement

https://doi.org/10.5194/egusphere-2024-1276
Preprint. Discussion started: 30 May 2024

different Manning's coefficient estimation methods in simulations. This feature enables users to select from various methods of roughness estimation, including not only a constant value but also methods dependent on the depth of runoff. Detailed information about these extensions can be found in the 'Code availability.' section. The elevation model is generated with a cell size of 1 × 1 meter, providing information about the gradient of each specific location in the database (Table 1). It's worth noting that micro depressions are considered by Manning's coefficient. At the outlet, located at the lower end of the terrain, discharge data is recorded for more analysis (Figure 1).

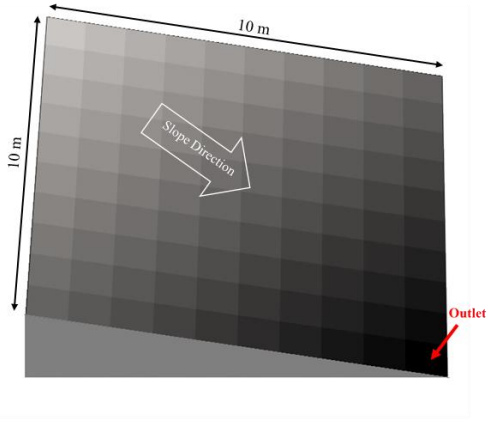

Figure 1: 1 × 1-meter digital elevation model applied for simulations, incorporating the specific slope of each site.

Time resolution was 1s and the total simulation time was chosen based on observation runoff data.

Overland flow is computed by the kinematic wave method. For the distributed routing of overland flow, a four-point finite-difference solution of the kinematic wave is together with Manning's equation (Jetten, 2002). To estimate the infiltration, Green-Ampt method was used (Rawls et al., 1983). This method contains variables that are measured in the field, porosity and the initial soil moisture content, or estimated by using the software package SPAW (Saxton and Willey, 2006), like as saturated hydraulic conductivity (Ksat) and average soil suction at the wetting front (Psi). Prior studies, including those by Jetten, (2002), Hessel et al. (2003) and Starkloff and Stolte (2014), have highlighted the primary sensitivity of OpenLISEM to Ksat and Psi parameters.

2.2 Surface roughness functions

The shape of a hydrograph is influenced by various factors related to rainfall, land characteristics, and drainage patterns. Therefore, by changing the Manning roughness coefficient, the shape of the output hydrograph changes. In this study, two depth-independent Manning's roughness coefficients and five depth-dependent roughness functions were introduced to OpenLISEM to quantify the effect of the vegetation on Manning's roughness coefficient.

2.2.1 Constant Manning's coefficients

The initial approach assumes a constant value for Manning's roughness coefficient based on Chow (1959), while in the other methods, the coefficient varies based on the water depth. The values of Manning's roughness coefficient using Chow's method for each site of the artificial rainfall experiments are given in Table 1.

In the study conducted by Feldmann et al., (2023), the Manning values were directly iterated within the framework they established. The authors reported that the most robust results, characterized by high Nash-Sutcliffe Efficiency (NSE) values, were achieved with constant Manning values, as presented in Table 1.

https://doi.org/10.5194/egusphere-2024-1276
Preprint. Discussion started: 30 May 2024

Table 1: Properties of experimental sites and the values of constant Manning's roughness coefficient.

Site*	Slope* %	Vegetation*	Veg_height* (m)	Plant coverage* %	soil type	n (Chow)	n (Feldmann)
1	12	Pasture	0.15	100	Clay	0.05	0.58
2	18	Pasture	0.1	100	Silty loam	0.05	0.60
3	**16**	**pasture**	**0.1**	**90**	**Loam**	**0.05**	**0.70**
4	**16**	**mustard**	**0.15**	**40**	**Clay loam**	**0.04**	**0.45**
5	**14**	**triticale (seeded)**	**0**	**0**	**Silty loam**	**0.03**	**0.18**
6	**21**	**pasture**	**0.05**	**100**	**Silty loam**	**0.04**	**0.65**
7	14	winter barley	0.3	80	Silty loam	0.05	0.38
8	**16**	**corn (seeded)**	**0.05**	**15**	**Sandy loam**	**0.035**	**0.13**
9	**21**	**pasture**	**0.1**	**100**	**Sandy loam**	**0.05**	**0.58**
10	32	pasture	0.15	100	Sandy clay loam	-	-
11	18	pasture	0.1	80	Silty clay	0.045	0.68
12	**19**	**pasture**	**0.15**	**100**	**Silty clay**	**0.05**	**0.65**
13	**11**	**alfalfa**	**0.2**	**40**	**Silty clay**	**0.04**	**0.28**
14	27	pasture	0.15	100	Silty clay	0.05	0.70
15	**14**	**winter barley**	**0.05**	**0**	**Clay loam**	**0.03**	**0.50**
16	**12**	**pasture**	**0.1**	**100**	**Clay loam**	**0.05**	**0.40**
17	**14**	**pasture**	**0.05**	**100**	**Silty loam**	**0.05**	**0.48**
18	**12**	**alfalfa and clover**	**0.2**	**60**	**Clay**	**0.045**	**0.38**
19	21	pasture	0.15	100	Sandy clay loam	0.05	0.98
20	9	corn (harvested)	0	0	Clay loam	0.03	0.05
21	14	green manure	0.15	50	Silty clay loam	0.04	0.35
22	12	pasture	0.2	100	Silty clay	0.05	0.38
23	14	corn (harvested)	0	0	Clay	0.03	0.08

* Data from Ries et al. (2020)

Pair sites

2.2.2 Linear method

Oberle et al. (2021) investigated flow depth-dependent roughness relationships using some experimental data on homogeneous artificial grass (Ruiz Rodriguez, 2017). Similar to Hinsberger et al. (2022), they found Strickler coefficient, k_{Str}, values varied with different water depths in the presence of grass. Based on their results, there are three zones to specify roughness within the data range, categorized according to the submergence ratio:

A linear function of relative submergence can be described for the roughness coefficient between emergent and fully submergence zones ($1 < \frac{h}{h_{veg}} < 5$ to 7) (Hinsberger et al. 2022).

These relationships are summarized in equation 1:

$$n_{Manning} = \begin{cases} \frac{k_{Str}}{5} & for\ \ 0 < h < h_{veg} \\ \frac{k_{Str}}{5} + k_{Str}\frac{h - h_{veg}}{5} & for\ h_{veg} < h < 5.h_{veg} \\ k_{Str} & for\ h > h_{veg} \end{cases} \quad (1)$$

In this study, the parameter Strickler's k is estimated based on the inverse of the roughness coefficient above the vegetation using Chow, (1959). Then Manning's coefficient is calculated from Eq.1, depending on the submergence ratio.

https://doi.org/10.5194/egusphere-2024-1276
Preprint. Discussion started: 30 May 2024

2.2.3 Luhar and Nepf's method

Another method to investigate vegetation effect on roughness was proposed by Luhar and Nepf (2013). They suggested the following relationships between the Manning roughness caused by vegetation and blockage factor, B_x, for both submerged and emergent vegetation.

$$n_{Manning-veg} = \begin{cases} \frac{Kh^{\frac{1}{6}}}{g^{\frac{1}{2}}} \left(\frac{C_f}{2}\right)^{\frac{1}{2}} (1-B_x)^{-\frac{3}{2}} & for\ h \le h_{veg} \text{ and } B_x < 0.8 \\ \frac{Kh^{\frac{1}{6}}}{g^{\frac{1}{2}}} \left(\frac{C_d a H}{2}\right)^{\frac{1}{2}} & for\ h \le h_{veg} \text{ and } B_x \ge 0.8 \\ \frac{Kh^{\frac{1}{6}}}{g^{\frac{1}{2}}} \frac{1}{\left(\frac{2}{C_f}\right)^{\frac{1}{2}} \left(1-\frac{h_{veg}}{h}\right)^{\frac{3}{2}} + \left(\frac{2}{C_d a h_{veg}}\right)^{\frac{1}{2}} \left(\frac{h_{veg}}{h}\right)} & for\ h > h_{veg} \end{cases} \quad (2)$$

where $n_{Manning-veg}$ is the vegetation component of Manning's n, a is the frontal area per unit volume parameter, C_d is the drag coefficient, C_f (= 0.015 - 0.19) is a coefficient to parameterize the shear stress at the interface between vegetated and unvegetated regions and the constant $K = 1\ \frac{m^{\frac{1}{3}}}{s}$ is required to make the equation dimensionally correct.

2.2.4 Exponential method

Feldmann et al., (2023) suggested an exponential correlation between the Manning coefficient and water depth (Eq. 3).

$$n = \frac{1}{c+e^{dh}} \quad (3)$$

This exponential equation describes the relationship between n and h in terms of the variables c and d. In this investigation, the optimum values of the c and d parameters, as calculated by Feldmann et al., (2023), are employed.

2.2.5 Kadlec's method

Based on experimental studies on shallow overland flow, Kadlec's power law was simplified by Jain et al., (2004) (Eq. 4).

$$n = n_0 \left(\frac{h}{h_0}\right)^{-\varepsilon} \quad (4)$$

where h_0 establishes the minimum flow depth, beyond which the roughness coefficient n_0 is assumed to remain constant. ε represents the influence of vegetation drag. The study utilized the optimal values for the parameters n_0 and ε as outlined in Feldmann et al., (2023). Nevertheless, they do not provide information on the h_0 value. Consequently, this parameter is assumed to be 5 times the plant height for each experimental site. This assumption is confirmed by previous studies (Hinsberger et al., 2022; Oberle et al., 2021).

2.2.6 Fu's equation

Fu et al., (2019) developed an equation to calculate Manning's n based on plant basal cover and flow depth (Eq. 5).

$$n = (a + b(1-e^{-0.061C_v})^{1.668}) h^{0.604-0.710e^{-0.219C_v}} \quad (5)$$

Where variable C_v is the ratio between the area covered by stems and the flume bed. It is considered as plant coverage in Ries et al. (2020). The parameters a and b vary with vegetation type. In this study, the values of a and b parameters obtained by Feldmann et al., (2023) are used.

All of these equations were incorporated into the source code of OpenLISEM in order to assess the impact of various roughness methodologies.

https://doi.org/10.5194/egusphere-2024-1276
Preprint. Discussion started: 30 May 2024

2.3 Study site

Ries et al. (2020). conducted 132 sprinkling experiments on natural hillslopes at 23 sites with different soil types and land use in Baden-Württemberg (Germany). The experiments conducted at Site 10 were not included in this analysis as they did not produce any runoff. Table 1 provides information about land use, vegetation properties, and soil characteristics for each site. The experimental area was a 10-meter-wide square, with slopes ranging from 9% to 32%. These experiments aimed to simulate a 100-year or locally observed maximum rainfall intensity event with different durations. The sequence of rainfall experiments commenced with Run.1 on the first day, which lasted for 60 minutes with a 100-year return period. Subsequently, Runs 2–4 were conducted on the following day, each lasting for durations of 60, 30, and 15 minutes, respectively, all with a 100-year return period. The experiments of the second day were concluded with Run.5, lasting for 180 minutes and representing an extreme scenario. Finally, on the third day, Run.6 was carried out, lasting for 60 minutes under an extreme scenario. Simultaneously, discharge at the outlet, rainfall intensity, and initial soil moisture were measured at a temporal resolution of 1 minute. Out of the 23 sites surveyed, 12 locations are paired sites, highlighted in bold in Table 1. This arrangement facilitates a direct comparison between the effects of two different land uses on runoff and infiltration. The deliberate choice of these paired sites is underscored by their proximity, with distances maintained within the threshold of less than 100 meters. To the comprehensive details of these experiments can be referred to Ries et al. (2020).

3 Calibration

To calibrate the model, the results of Run.2 of the rainfall experiment for all sites was used, except for sites 1 and 14. In site 1, Run. 4 represents results for rainfall 100 years and a duration 60 minutes. Since Run. 2 in site 14 does not have any runoff, Run.6 is selected for calibration. The reason for choosing Run. 2 for calibration was that the soil moisture conditions during this test were neither excessively dry nor fully saturated. Additionally, the duration of the rainfall was moderate, indicating an average condition. Therefore, Run. 2 is more representative of the soil conditions expected in the study area. In this study, our calibration efforts were exclusively directed toward the Ksat and Psi parameters due to the sensitivity of the model to these specific parameters.

The parameter space was sampled with 5000 parameter sets drawn from Latin Hypercube Sampling with SPOTPY (Statistical Parameter Optimization Tool), an open-source Python package developed by Houska et al., (2015). For this process, the range considered for Ksat values spanned from 0.5 to 100, while the range for Psi extended from 0.25 to 3 times the initial value. The objective function to calibrate is the max value of Nash Sutcliff efficiency (NSE) which is commonly used to assess the performance of hydrological models (Nash and Sutcliffe, 1970).

Once the calibration process was completed, we determined the optimal Ksat and Psi values for each site and roughness method based on the best result of NSE. Figure 2 displays a framework illustrating the calibration and simulation process of models.

Furthermore, to investigate whether calibrating Manning's n alongside Ksat and Psi can lead to improved model performance or not, we repeat the calibration with three parameters: K_{sat}, Psi, and Manning's n. It is referred to as "3-parameter" in this paper. Using this method helps us to understand the effect of interactions among calibrated parameters on model performance.

After calibrating the values of Ksat and Psi for each site and roughness method, the model validation is conducted for the remaining experiments: Run. 1 and Run. 3 through 6. Key performance metrics including NSE, percentage bias, and Kling-Gupta efficiency are computed to provide a thorough assessment of the model's performance and validation. The results from various analyses are compared with the measured runoff values, facilitating the assessment of the different roughness methods. Additionally, by comparing the results for paired sites, it is possible to investigate the impact of vegetation cover on overland flow.

https://doi.org/10.5194/egusphere-2024-1276
Preprint. Discussion started: 30 May 2024

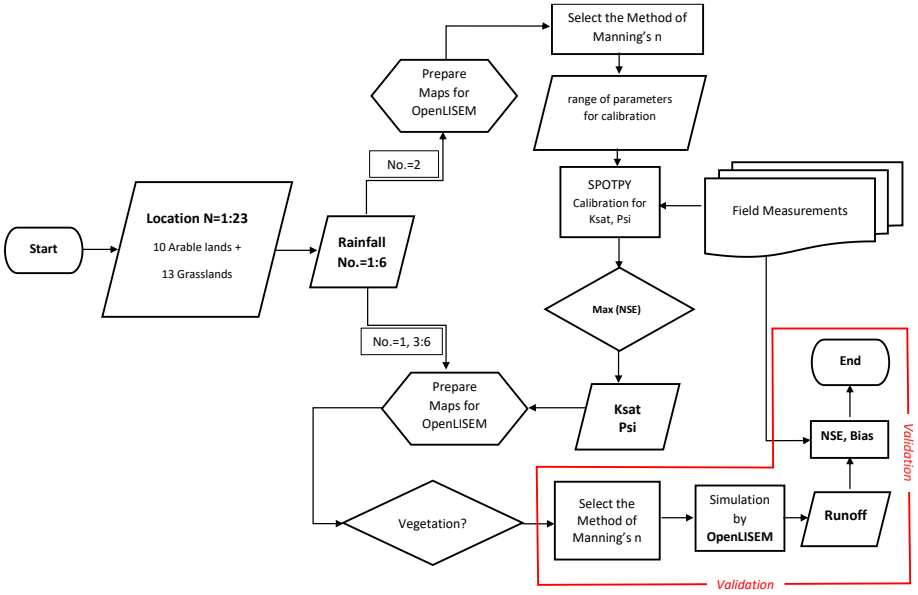

195 **Figure 2: Framework for calibration and validation of the models.**

4 Result

4.1 Calibration of different roughness methods

Regarding the calibration using various Manning's coefficient methods, the hydrograph from the calibration generally matches well with the observed hydrograph at most of the locations. For example, Figure 3 shows the different calibrated hydrographs
200 in site 6 with the measured hydrograph. The calibrated hydrographs closely resemble the patterns seen in the measured hydrograph. The NSE values for calibration at this location have a range of 0.7-0.9. The NSE values from calibration results for all sites are outlined in Table 2, featuring color-coded representations. NSE values below 0.35 are highlighted in dark gray, those between 0.35 and 0.75 in mild gray, and values exceeding 0.75 in light gray. Fu's method exhibited inadequate calibration outcomes for sites 5, 15, 20, and 23, indicated by negative NSE values. The unfavorable calibration results were observed in
205 site 16 with the 3-parameter method, represented in Table 2. Conversely, all other methods yielded satisfactory results. Excluding the dark gray cells, the calculated NSE values maintained a high average of 0.86 across other cells, underscoring their acceptable performance.

https://doi.org/10.5194/egusphere-2024-1276
Preprint. Discussion started: 30 May 2024

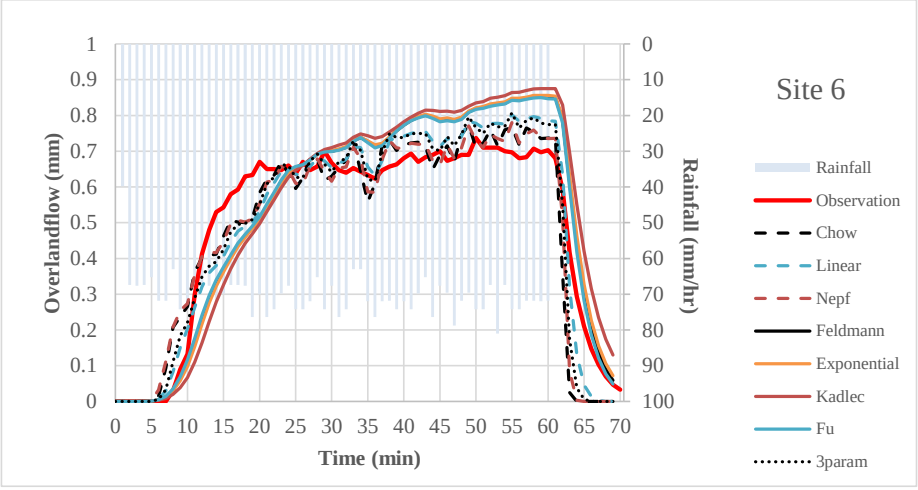

Figure 3: Comparison of the hydrograph computed using OpenLISEM with various roughness coefficient methodologies against the observed discharge.

Table 2: Maximum model performance (Nash-Sutcliffe-Efficiency) for parameters calibration of the different roughness models, separated for each site. Rainfall simulation run 2 has been used for calibration, except for sites 1 and 14 (see section 3). The grey scale indicates the NSE value with values below 0.35 in dark grey and 1 as white.

Site No	Run No	NSE							
		Chow	Linear	Nepf	Feldmann	Exp	Kadlec	Fu	3-param
1	run4*	0.88	0.84	0.88	0.68	0.76	0.29	0.84	0.88
2	run2	0.71	0.74	0.71	0.75	0.76	0.76	0.76	0.67
3	run2	0.82	0.89	0.84	0.90	0.91	0.91	0.91	0.67
4	run2	0.87	0.94	0.90	0.95	0.94	0.94	0.94	0.73
5	run2	0.98	0.98	0.99	0.93	0.92	0.95	-5.80	0.98
6	run2	0.87	0.91	0.89	0.82	0.81	0.72	0.84	0.81
7	run2	0.87	0.92	0.89	0.91	0.76	0.92	0.87	0.67
8	run2	0.93	0.87	0.94	0.89	0.90	0.94	0.80	0.92
9	run2	0.81	0.94	0.83	0.99	0.99	0.99	0.99	0.71
11	run2	0.78	0.87	0.79	0.95	0.96	0.94	0.90	0.66
12	run2	0.78	0.95	0.86	0.95	0.90	0.91	0.95	0.31
13	run2	0.77	0.86	0.81	0.87	0.88	0.80	0.86	0.30
14	run6*	0.96	0.97	0.97	0.90	0.85	0.92	0.96	0.96
15	run2	0.72	0.73	0.76	0.83	0.67	0.84	-4.04	0.70
16	run2	0.03	0.41	0.02	0.26	0.05	0.47	0.54	-26.65
17	run2	0.85	0.94	0.87	0.96	0.96	0.95	0.96	0.68
18	run2	0.69	0.81	0.75	0.85	0.86	0.88	0.88	0.64
19	run2	0.69	0.83	0.71	0.97	0.97	0.97	0.97	0.55
20	run2	0.92	0.93	0.94	0.94	0.94	0.94	-5.41	0.86
21	run2	0.88	0.97	0.93	0.96	0.94	0.97	0.71	0.75
22	run2	0.95	0.88	0.95	0.80	0.80	0.19	0.84	0.92
23	run2	0.98	0.98	0.98	0.97	0.95	0.96	-5.54	0.98

The bias percentage is computed for each hydrograph, utilizing the calibrated Ksat and Psi values, as detailed in Table 3. Analogous to the NSE values, the location 16 exhibits the highest bias percentage using the 3-parameter method. Additionally, employing the Fu equation for locations 5, 15, 20, and 23 yields a bias percentage of -100. In the remaining cells of the table,

https://doi.org/10.5194/egusphere-2024-1276
Preprint. Discussion started: 30 May 2024

a transition from darker gray to lighter gray indicates bias percentages approaching zero. A more significant deviation from zero suggests that the calibration process is not well-executed.

Table 3: Percentage of Bias values for parameters calibration of the different roughness models, separated for each site. Rainfall simulation run 2 has been used for calibration, except for sites 1 and 14 (see section 3). The grey scale indicates the absolute pBias value with values above 100% in dark grey and no bias as white.

Site No	Run No	pBias							
		Chow	Linear	Nepf	Feldmann	Exp	Kadlec	Fu	3-param
1	run4*	8.04	5.73	2.08	12.03	9.12	22.42	4.09	1.08
2	run2	-11.96	-9.51	-10.96	-8.24	-8.30	-5.34	-7.08	-3.29
3	run2	-11.16	-8.79	-10.15	-5.97	-4.97	-4.72	-4.85	13.95
4	run2	-5.15	-4.69	-4.96	-0.30	1.25	-5.09	0.78	12.33
5	run2	-0.55	-0.20	-0.09	2.22	2.85	1.22	-100.00	0.16
6	run2	-2.54	0.26	-2.21	6.76	7.11	8.85	6.51	7.14
7	run2	-2.20	-0.13	-1.87	1.60	9.36	-1.35	4.77	19.43
8	run2	-1.10	0.94	-1.26	0.82	1.10	-0.95	-2.16	3.89
9	run2	-6.96	-3.45	-6.16	-0.58	0.78	-0.77	1.13	3.94
11	run2	-14.17	-11.09	-13.76	-5.43	-1.86	-4.56	-10.16	10.58
12	run2	-2.57	1.07	-6.29	5.35	10.61	7.70	-2.14	52.67
13	run2	-0.98	-1.75	0.01	1.32	1.31	0.23	2.31	35.06
14	run6*	-0.58	-0.33	0.37	5.94	8.29	3.28	1.23	-5.39
15	run2	-0.93	-1.81	-1.56	7.94	9.73	3.53	-100.00	3.23
16	run2	9.56	4.78	15.01	15.87	19.89	1.53	4.68	326.29
17	run2	-8.47	-3.18	-7.57	-1.10	0.22	-0.97	-2.16	15.64
18	run2	-12.10	-9.36	-12.56	-7.54	-5.68	-4.64	-4.54	4.01
19	run2	-7.43	-4.52	-7.11	-0.15	-0.10	-0.04	-0.02	5.14
20	run2	-2.89	-2.94	-2.45	-2.72	-2.22	-2.53	-100.00	4.94
21	run2	-4.93	-1.90	-3.27	0.70	0.31	-2.07	-5.83	3.86
22	run2	1.62	5.41	1.31	7.51	7.18	12.29	6.46	-1.23
23	run2	-0.16	-0.40	0.19	0.49	0.87	1.02	-100.00	-0.54

Site 16 displayed a comparatively lower NSE compared to other locations, while the remaining monitoring sites demonstrated effective calibration. At site 16, the recorded runoff is exceptionally low, with a cumulative measurement of only 1.049 mm, while the target intensity of rainfall is 69.3 mm/hr. These low runoff values pose a significant challenge for model calibration, resulting in a relatively lower NSE score compared to other sites. Figure 4 and Figure 5 display the calibrated values of saturated hydraulic conductivity and average soil suction at the wetting front, respectively, calculated using different methods across all sites. Notably, in Fu's method, the values of Ksat for sites 20 and 23 significantly differ from those obtained with other methods. Similarly, the values of Psi for sites 5 and 15 exhibit notable differences compared to values obtained through other methods.

https://doi.org/10.5194/egusphere-2024-1276
Preprint. Discussion started: 30 May 2024

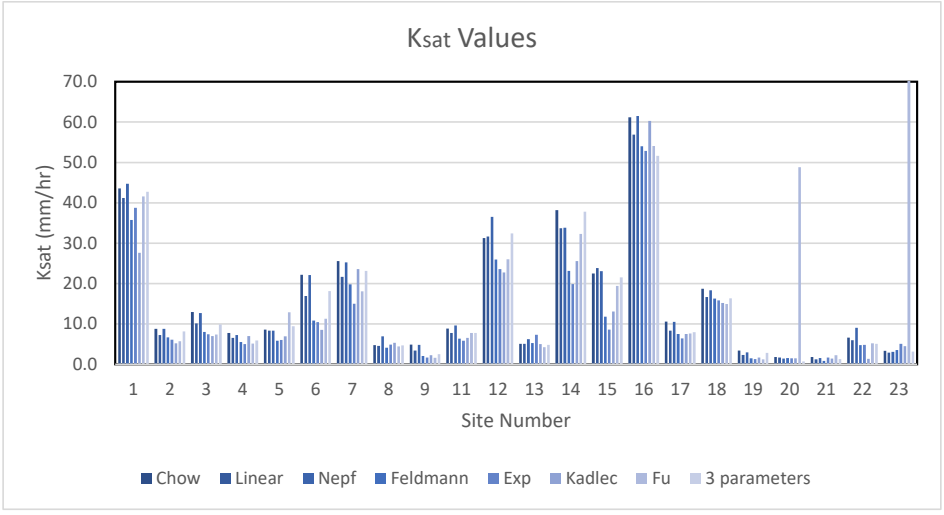

Figure 4: Different values of calibrated Ksat for various roughness estimation methods.

235

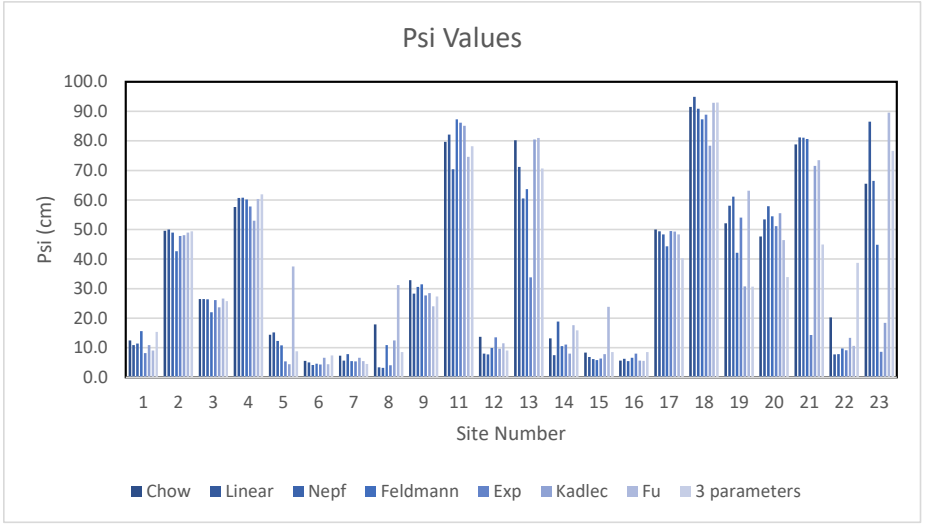

Figure 5: Different values of calibrated Psi for various roughness estimation methods.

240 **4.2 Validation of different roughness methods**

After calibrating the Ksat and Psi, models were developed for the rest experiments. We calculated NSE and bias parameters to assess its performance for each model. The simulations were iteratively repeated, considering all methods of roughness estimation. A total of 104 models were simulated, each corresponding to different sites or rainfalls. However, models associated with Run.2 and 3 at Site 14, as well as Run.1 at Sites 12 and 16, were excluded from our investigation due to the
245 absence of runoff in these specific experiments. The outcomes reveal that the maximum NSE range is 0.97-0.99 for different methods. Depending on the type of method, the number of models with negative NSE varies between 27 and 43. In these cases, the model has not performed well. Given that negative NSE values indicate the inefficiency of the model in simulating runoff,

https://doi.org/10.5194/egusphere-2024-1276
Preprint. Discussion started: 30 May 2024

we focused our investigation on the distribution of positive NSE values by excluding these underperforming models. Figure 6 illustrates the distribution of NSE for values greater than zero. On the other hand, Chow, Nepf, constant n of Feldmann, Exponential, Kadlec, Fu, and the 3-parameter methods have 29, 35, 17, 12, 20, 10, and 28 models, respectively, with NSE values greater than 0.8. The Linear method stands out with the maximum number of models, 37, having NSE greater than 0.8. In these cases, the model has performed excellently.

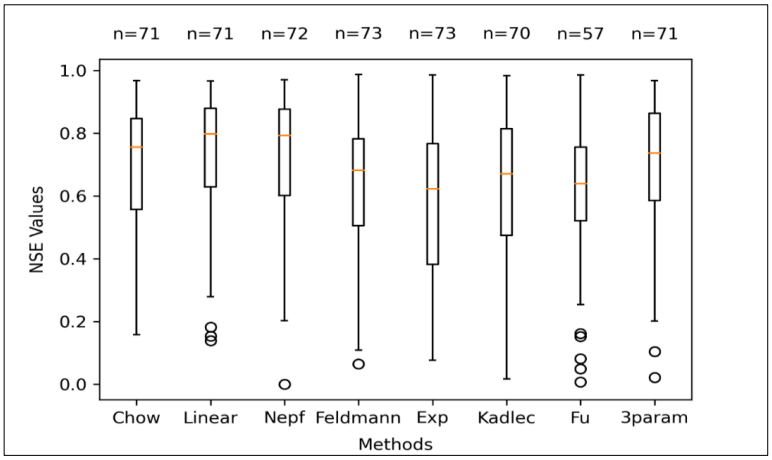

Figure 6: Distribution of the absolute values of NSE for each method of roughness for the validation runs.

The percentage bias results for the simulated hydrograph compared to the measured hydrograph exhibit a broad range from -100% to 100%. Notably, methods such as Feldmann, Exp, and Kadlec have 12 models with biases exceeding 100%. The Linear and 3-parameter methods each account for 10 such models, while Nepf and Fu methods have 9 models each. The Chow method is associated with 8 models exhibiting a bias greater than 100%. For a clearer representation, Figure 7 focuses on the percentage bias results within the range of -100% to 100%. Based on the analysis presented in Figure 7, it is evident that all the methods exhibit almost a consistent trend, with the majority showcasing model bias consistently below zero. This suggests a systematic underestimation across various roughness estimation techniques.

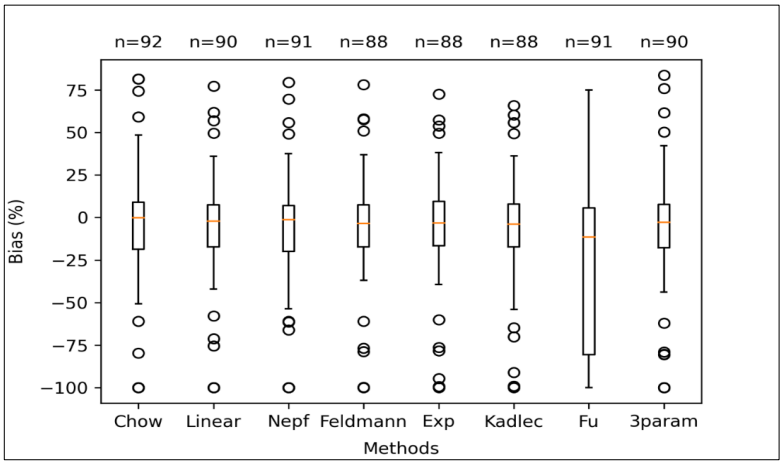

Figure 7: Distribution of the percentage bias for each method of roughness for the validation runs.

https://doi.org/10.5194/egusphere-2024-1276
Preprint. Discussion started: 30 May 2024

To classify the simulation results, NSE criteria established by Motovilov et al., (1999) are applied, as outlined in Table 4. Additionally, bias percentage values are interpreted based on the criteria in Table 4. High positive NSE values (close to 1) indicate that the model's predictions are in excellent agreement with the observed data.

Table 4: Criteria of NSE value (Motovilov et al., 1999) and Bias.

NSE value	Bias% value	Interpretation
0.75<NSE	-10%<Bias<10%	Good
0.36<NSE<0.75	-50%<Bias<-10% or 10%<Bias<50%	Qualified
NSE<0.36	Bias<-50% or 50%<Bias	Not-Qualified

The analysis reveals that the Nepf, Linear, and Chow methods exhibit the most favorable performance, with 44, 42, and 38 models falling into the "Good" category based on NSE values. Conversely, for the 3-parameter, Kadlec, constant n by Feldmann, exponential, and Fu methods, 33, 26, 25, 22, and 15 models respectively meet the "Good" NSE criteria. Interestingly, bias values across different methods are relatively comparable. Linear, Kadlec, Nepf, and Chow demonstrate particularly robust performance, each with 42, 40, 39, and 39 models falling within the -10% to 10% bias range. This consistency in bias values suggests a commendable performance by these models based on bias percentage criteria.

The validation results of the models are visually presented in Figure 8 and Figure 9, highlighting their adherence to both NSE and bias criteria. These figures provide a comprehensive overview of the model's performance, emphasizing the importance of considering both NSE and bias values for a thorough evaluation of simulation outcomes. The comparison of these criteria aids in discerning the models that not only achieve high efficiency in reproducing observed data (NSE) but also demonstrate minimal bias in their predictions.

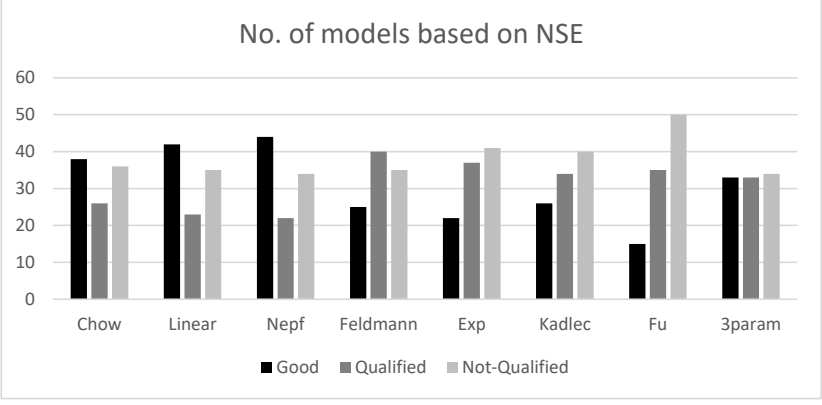

Figure 8: Distribution of the percentage bias for each method of roughness estimation.

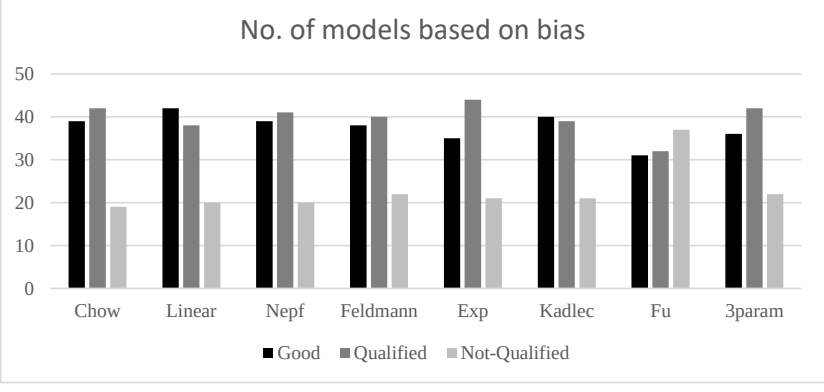

Figure 9: Distribution of the percentage bias for each method of roughness estimation.

https://doi.org/10.5194/egusphere-2024-1276
Preprint. Discussion started: 30 May 2024

285 To provide further insight, Figure 10 illustrates a comparison of the simulated falling limb of hydrographs using different roughness estimation methods for all experiments conducted at site 9. Site 9 is specifically chosen because its hydrographs were featured in Feldmann et al.'s, (2023) study, and the calibration for the four methods employed therein is superior to that of the Linear and Nepf methods, as depicted in Table 2. Figure 10 demonstrates that Kadlec, Feldmann, Exponential, and Fu methods approximate the falling limb of the hydrograph more closely to the observed hydrograph compared to the Linear,
290 Nepf, and Chow methods. It's essential to note that the base of optimization in Feldmann et al., (2023) study is on the falling limb of the hydrograph, where it shows superior performance. However, the NSE results for the entire hydrograph are better for Nepf, Linear, and Chow.

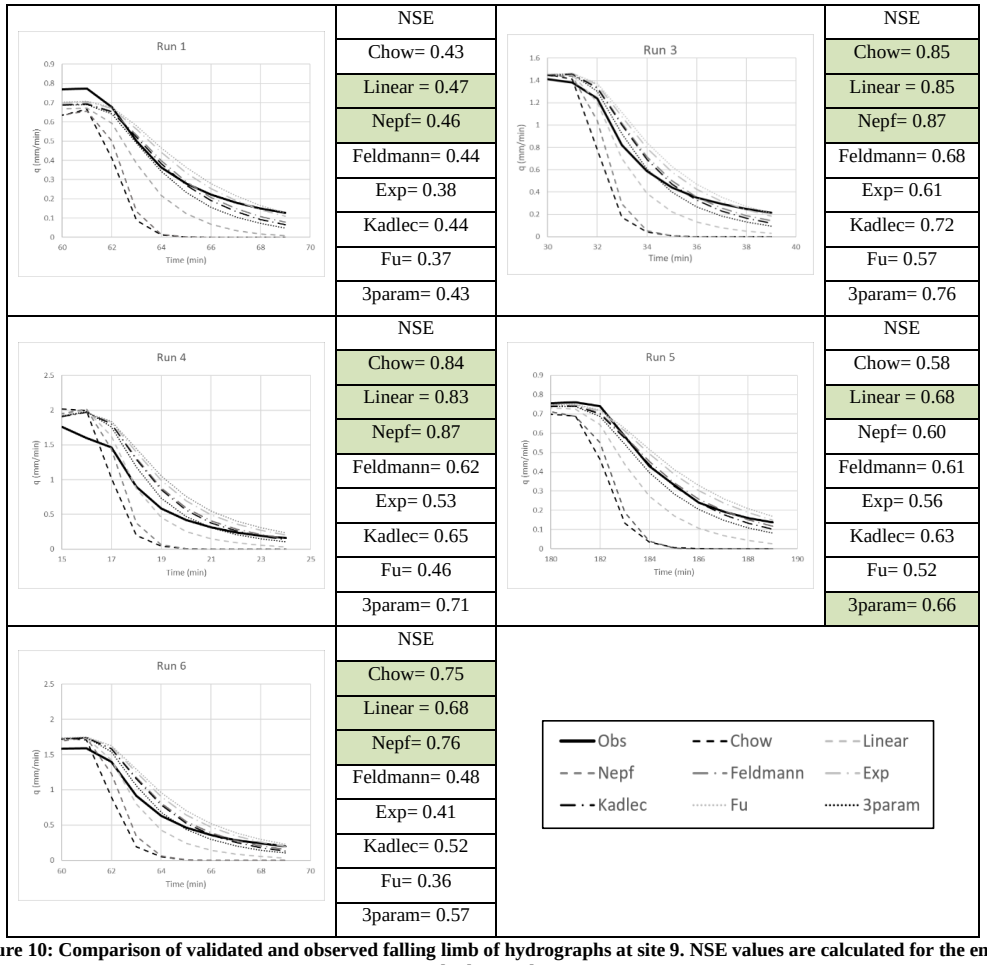

Figure 10: Comparison of validated and observed falling limb of hydrographs at site 9. NSE values are calculated for the entire
295 **hydrograph.**

4.3 Effect of initial condition and pre-event soil moisture

The validation outcomes of the roughness methods revealed a notable association between most models exhibiting NSE values below zero and Runs.1 and 5, with frequencies of approximately 50% and 30%, respectively. For example, among the 28
300 models exhibiting negative NSE values in the Nepf method, 12 and 8 models correspond to Runs.1 and 5, respectively, suggesting unsatisfactory performance compared to the other runs. Bias analysis reveals that most models in Run.5 exhibit

https://doi.org/10.5194/egusphere-2024-1276
Preprint. Discussion started: 30 May 2024

negative bias, indicating a tendency to underestimate runoff. Conversely, most models in Run.1 show positive bias, indicating a tendency to overestimate runoff.

Exploring the underlying reasons for these observations' sheds light on the impact of initial soil moisture conditions on model performance. In Run.1, soil conditions during the rainfall experiment exhibited lower moisture levels compared to subsequent runs. This difference is attributed to the drier state of soil moisture in Run.1 compared to Run.2, which was utilized for calibration. Notably, the duration and target intensity of these two runs are similar. Consequently, the majority of locations within Run.1 experienced minimal runoff occurrences due to the diminished soil moisture content. This phenomenon resulted in Run.1 exhibiting the least favorable performance on average, as indicated by the evaluation outcomes. In contrast, the soil conditions in the other runs were characterized by higher moisture levels, influenced by the retention of moisture from preceding runs. For Run.5, despite the rainfall intensity being similar to Run.2, the rainfall duration is three times longer, implying distinct soil moisture conditions during the experiment. According to Ries et al., (2020), Run.2 was conducted as the first experiment on the 3rd day, while Run.5 was the 4th experiment on the same day. This sequential rainfall event may affect infiltration. Antecedent moisture conditions, representing soil moisture content before rainfall events, can impact runoff. Therefore, most of Run.6, as a first experiment on 5th day with higher intensity, showed a lower mean surface runoff coefficient compared to Run.5 in the study by Ries et al., (2020).

4.4 Result of different vegetation coverage

The spatial proximity between the paired experimental sites offers a unique advantage in the research, providing an environment where variations in soil characteristics can be minimized, enhancing the validity of the comparative analysis. In Figure 11, a comparative analysis between vegetation cover and Ksat, as determined by the Chow method, is presented. Except for sites 17 and 18, which feature different soil types, making them non-comparable, the remaining pairs reveal an increase in Ksat corresponding to more vegetation coverage. Notably, the contrast in Ksat is particularly pronounced between sites 15 and 16. Site 15, characterized as devoid of vegetation cover, displays a stark difference from site 16, boasting 100% vegetation coverage. The calibration results underscore this disparity, indicating a substantial Ksat difference of approximately 60 mm/hr. Conversely, for sites 8 and 9, this difference in Ksat is minimum. Specifically, for the Chow method, the values are nearly identical for these two sites. Considering alternative roughness methods, it becomes apparent that the Ksat of site 9 is marginally lower than that of site 8, despite site 9 featuring a higher level of vegetation. It's noteworthy that, although Ksat values may show only slight differences, another critical parameter influencing infiltration, Psi, exhibits a substantial contrast between sites 8 and 9, as displayed in Figure 5. Specifically, Psi is higher for site 9 than site 8, resulting in an enhancement in infiltration. This highlights the relationship between various parameters and their combined impact on the overall dynamics of infiltration.

https://doi.org/10.5194/egusphere-2024-1276
Preprint. Discussion started: 30 May 2024

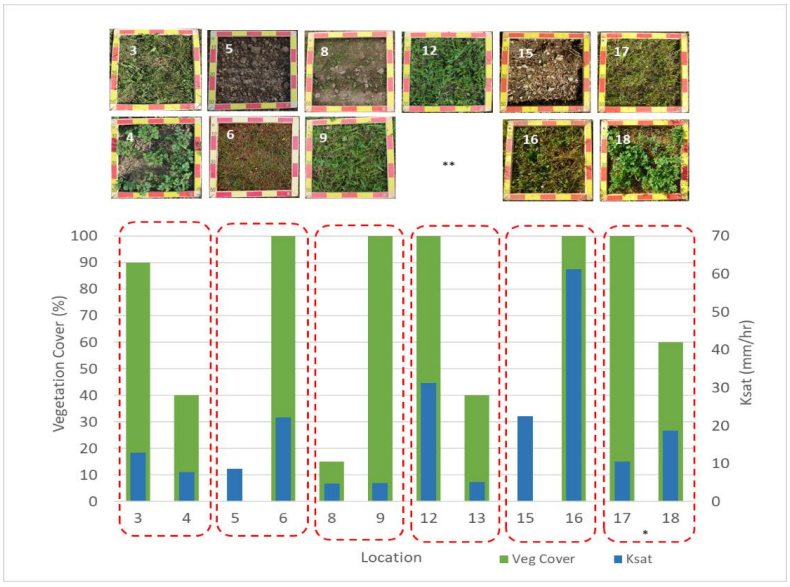

Figure 11: Saturated hydraulic conductivity values for various land uses in paired sites. * Sites 17 and 18 are not comparable because of different types of soil. ** The vegetation cover images are from Ries et al., (2020). There is no picture for Site 13.

5 Discussion

5.1 Validation of different roughness methods

Our study on validation of different roughness estimation methods demonstrated that the models constructed using Fu's function display weaker simulation results compared to alternative methods. This aligns with Feldmann et al. 's, (2023) findings, who observed that Fu's equation tends to yield lower NSE values, primarily due to the limited adaptability of the formula. Furthermore, they noted that significantly lower results, in comparison to Kadlec's Power Law, are obtained on sites where roughness visibly decreases with water depth. Linear, Chow, and Nepf, in that sequence, demonstrate the highest frequency of models exhibiting good performance in evaluating the hydrograph of runoff. Subsequent calibrations with the 3-parameter and then the Kadlec method showcase improved performance compared to the Exponential and Fu's formula. These findings are consistent with the results of Feldmann et al. 's, (2023) study, supporting the overall superiority of Kadlec's Power Law over the Exponential and Fu methods on average. Feldmann et al., (2023) attribute the enhanced performance of Kadlec's formula to its superior reflection of vegetation variability, effectively capturing the nuances associated with increasing or decreasing roughness.

The experimental study on vegetated surfaces conducted by Hinsberger et al., (2022) shows that roughness is significantly influenced by water depth. They emphasize the importance of considering water depth-related roughness for precise catchment modeling. However, our findings indicate that the deviation in Manning's n value recommended by Chow is not substantial when the model is calibrated. Employing the Linear and Nepf relationship for estimating roughness can enhance accuracy. This concurs with previous studies advocating for roughness determination based on the degree of vegetation submergence (Hinsberger et al., 2022; Scheres et al., 2020; Wilson and Horritt, 2002). Wilson and Horritt, (2002) concluded that Manning's n increases significantly as the flow depth approaches the depth of vegetation, converging towards a consistent value at higher levels of submergence. This trend aligns with hydraulic behavior explained by Oberle et al., (2021) and Luhar and Nepf, (2013).

On the other hand, the comparison with Exponential and Kadlec's equations reveals more deviation. In Feldmann et al.'s, (2023) assessment of roughness methods, including Kadlec, Feldmann's constant Manning, Fu, and exponential, stand out for

https://doi.org/10.5194/egusphere-2024-1276
Preprint. Discussion started: 30 May 2024

providing a more robust roughness solution, particularly based on the falling limb of the hydrograph when infiltration remains nearly constant. However, our findings indicate that vegetation not only influences roughness coefficient values but also impacts saturated hydraulic conductivity, thus affecting infiltration dynamics. Our results reveal that the roughness values derived from Feldmann et al.'s, (2023) approach exhibit more significant variation compared to other methods, potentially due to its neglect of the vegetation's effect on infiltration.

5.2 Effect of initial condition and pre-event soil moisture

The pivotal role of antecedent conditions in shaping a catchment's response to rainfall events has been extensively discussed in the literature. Beven, (2012) underscores the significance of antecedent conditions in determining the mechanisms governing catchment response. Our study delves into this aspect, revealing notable discrepancies in model outcomes between different runs, particularly evident in Runs.1 and 5. In Run.5, characterized by intense rainfall events following Runs 2-4, and Run 1, where initial soil moisture conditions were notably drier compared to other runs, we observed considerable deviations from measured data. This inconsistency echoes findings from Feldmann et al., (2023), who explored the influence of rainfall intensity on roughness variability. Notably, they observed a decrease in median deviation from the roughness mean in Run.5 during longer rain events, suggesting a potential influence of flow path formation on roughness values. However, in Run.6, the deviation from the mean increased once more, indicating it may be due to antecedent rainfall's impact on runoff response rather than the effect of rainfall intensity on roughness. The discrepancy in antecedent rainfall between Run 2, used for calibration, and Runs 1 and 5, which experienced extreme soil moisture conditions, likely contributed to the divergent validation results. Previous research, including studies by Zehe et al., (2010); Zwartendijk et al., (2023); Tobón and Bruijnzeel, (2021), highlights the profound impact of antecedent wetness conditions on runoff behavior. Brocca et al., (2008) emphasized the influence of initial soil moisture conditions on runoff characteristics, further corroborating our findings.

Our study suggests that infiltration and runoff dynamics during extreme events, such as those observed in Run.5, may be significantly influenced by antecedent rainfall. This aligns with existing literature indicating the crucial role of antecedent conditions in modulating runoff depth and coefficients. Castillo et al., (2003) observations underscore the dominance of infiltration excess overland flow during intense rainfall events or in less permeable soils, emphasizing the influence of initial soil moisture conditions on runoff responses. The limitations of the applied infiltration model, particularly evident under extreme soil moisture conditions, warrant attention. The Green-Ampt method's assumption of initially dry soil may not accurately capture infiltration dynamics during extreme rainfall events when the soil is near saturation. This highlights the need for improved models that account for varying antecedent conditions to enhance predictive accuracy. The findings of Zehe and Blöschl, (2004) further underscore the challenges in predicting hydrological responses accurately, particularly under uncertain initial soil moisture conditions. While extreme states, extremely dry or wet, exhibit better predictability, intermediate values pose challenges due to threshold processes governing the transition from matrix to macropore flow. However, the results of our study indicate that extreme states show poor predictability in hydrological response. This indicates that understanding the interaction between rainfall attributes and antecedent wetness is essential for accurately predicting runoff responses. Similarity in soil moisture conditions between the validation and calibration models may cause in more accurate outcomes. However, Zehe and Blöschl, (2004) stated, despite assuming perfect knowledge of the processes involved, the extent to which one can measure initial conditions in detail, combined with the inherent nonlinearity of the system, imposes constraints on both the repeatability of experiments and the predictability of models.

https://doi.org/10.5194/egusphere-2024-1276
Preprint. Discussion started: 30 May 2024

5.3 Result of different vegetation coverage

The findings presented in our study validate previous research, which has emphasized the significant differences in near-surface saturated hydraulic conductivity across various land covers (Zwartendijk et al., 2023). These differences result in different shaping perched water table dynamics and overland flow responses (Ghimire et al., 2020; van Meerveld et al., 2021; Zwartendijk et al., 2020, 2023). The study conducted by Wu et al., (2024) on the temporal variability of Ksat throughout the growing season revealed the significant influence of root growth. It seems, that due to the root growth and consequent improvement in soil pore connectivity, there is an increase in Ksat. Consequently, top-soil infiltration rates typically experience improvement, resulting in reduced overland flow and a decrease or delayed runoff response to rainfall events (van Meerveld et al., 2019). Jarvis et al., (2013) identified land use as one of the top three most significant predictors for Ksat. Intensive cultivation of arable land significantly diminishes topsoil hydraulic conductivity compared to perennial agriculture, natural vegetation, and forests, by approximately 2–3 times. They attributed this reduction to the disruptive effects of tillage on macropores, including faunal and root biopores.

Our research indicates that in the presence of vegetation, not only is surface roughness important in hydrological processes, but the increase in Ksat also significantly influences the response of hydrological models to runoff. This highlights the critical importance of incorporating vegetation-induced changes in hydraulic conductivity when modeling runoff responses. A great difference to the related studies by Feldmann et al., (2023)and Hinsberger et al., (2022) is the use of a model with an integrated infiltration model. Classical engineering models for surface runoff like HEC-RAS and most commercial models deal with infiltration as a process that can be determined a priori and subtracted directly from the rainfall. But the ability of the soil to absorb water is dynamic in its nature and often oversimplified and inaccurate (Beven, 2021). In our investigation, we utilized the dynamic Green-Ampt Infiltration model from OpenLISEM, and we managed to replicate the infiltration process in the majority of cases. However, while we observe the strong effect of vegetation on infiltration capacity, our data set is not sufficient to come up with a robust estimate to quantify this effect.

6 Conclusion

Our study provides the evaluation of various roughness estimation methods and their impact on hydrological modeling using OpenLISEM. Through model calibration and validation, we have gained valuable insights into the performance of each roughness method. Our findings reveal that certain methods, such as Linear, constant Manning's n proposed by Chow, and the physical base method proposed by Luhar and Nepf (2013), demonstrate favorable performance in reproducing observed hydrological data, as evidenced by high NSE values and minimal bias. Methods like Fu's equation exhibit weaker simulation results, attributed to its limited adaptability and lower NSE values.

Our study highlights the significance of incorporating vegetation-induced changes in hydraulic conductivity when modeling runoff responses. We observed notable differences in near-surface saturated hydraulic conductivity across various land covers. The differences observed in model outcomes between various runs in one site highlight the need for improved models that accurately account infiltration for varying antecedent conditions. Surface runoff models use vegetation solely as a parameter of surface roughness and rainfall runoff models as a transpiration parameter. For the effect of storm events in developed landscapes, vegetation is an important regulator of infiltration, yet this effect is not well represented in current models. Future studies should investigate which rainfall events yield better results when included in the calibration process. Selecting the most representative rainfall event should consider both dry and saturated soil moisture conditions, enhancing the accuracy of hydrological modeling.

https://doi.org/10.5194/egusphere-2024-1276
Preprint. Discussion started: 30 May 2024

Code availability.

https://github.com/philippkraft/openlisem/tree/modified_manning_console

Author contributions. AM: Programming, Simulation, Data analysis, Manuscript draft writing.

PK: Conceptualization, Funding acquisition, Software development, Manuscript review and editing.

Competing interests. The authors declare that they have no conflict of interest.

Acknowledgements. This research was funded by Hessisches Landesamt für Naturschutz, Umwelt und Geologie (HLNUG) for the project "Innovativer Erosionsschutz für Hessen unter Klimawandel" (Z1-15C c 01.02.).

References

Aberle, J. and Järvelä, J.: Hydrodynamics of Vegetated Channels, in: Rivers – Physical, Fluvial and Environmental Processes, edited by: Rowiński, P. and Radecki-Pawlik, A., Springer International Publishing, Cham, 519–541, https://doi.org/10.1007/978-3-319-17719-9_21, 2015.

Beven, K.: Rainfall-Runoff Modelling: The Primer, 1st ed., Wiley, https://doi.org/10.1002/9781119951001, 2012.

Beven, K.: The era of infiltration, Hydrol. Earth Syst. Sci., 25, 851–866, https://doi.org/10.5194/hess-25-851-2021, 2021.

Brocca, L., Melone, F., and Moramarco, T.: On the estimation of antecedent wetness conditions in rainfall–runoff modelling, Hydrol. Process., 22, 629–642, https://doi.org/10.1002/hyp.6629, 2008.

Castillo, V., Gomezplaza, A., and Martinezmena, M.: The role of antecedent soil water content in the runoff response of semiarid catchments: a simulation approach, J. Hydrol., 284, 114–130, https://doi.org/10.1016/S0022-1694(03)00264-6, 2003.

Chow, V. T.: Open-Channel Hydraulics, McGraw-Hill Book Co., NY, USA, 110 pp., 1959.

Dalledonne, G. L., Kopmann, R., and Brudy-Zippelius, T.: Uncertainty quantification of floodplain friction in hydrodynamic models, Hydrol. Earth Syst. Sci., 23, 3373–3385, https://doi.org/10.5194/hess-23-3373-2019, 2019.

D'Ippolito, A., Calomino, F., Alfonsi, G., and Lauria, A.: Flow Resistance in Open Channel Due to Vegetation at Reach Scale: A Review, Water, 13, 116, https://doi.org/10.3390/w13020116, 2021.

Feldmann, D., Laux, P., Heckl, A., Schindler, M., and Kunstmann, H.: Near surface roughness estimation: A parameterization derived from artificial rainfall experiments and two-dimensional hydrodynamic modelling for multiple vegetation coverages, J. Hydrol., 617, 128786, https://doi.org/10.1016/j.jhydrol.2022.128786, 2023.

Freeman, G. E., Rahmeyer, W. H., and Copeland, R. R.: Determination of Resistance Due to Shrubs and Woody Vegetation, US Army Corps of Engineers, Engineer Research and Development Centre Report, 2000.

Fu, S., Mu, H., Liu, B., Yu, X., and Liu, Y.: Effect of plant basal cover on velocity of shallow overland flow, J. Hydrol., 577, 123947, https://doi.org/10.1016/j.jhydrol.2019.123947, 2019.

Ghimire, C. P., Zwartendijk, B. W., Ravelona, M., Lahitiana, J., and Van Meerveld, H. J.: Hydrological and meteorological data for three plots with different vegetation near Andasibe, Madagascar, 2014-2015, https://doi.org/10.5285/5D080FEF-613A-4F24-A613-B249CCDD12BF, 2020.

Green, J. C.: Modelling flow resistance in vegetated streams: review and development of new theory, Hydrol. Process., 19, 1245–1259, https://doi.org/10.1002/hyp.5564, 2005.

Hessel, R., Jetten, V., Liu, B., Zhang, Y., and Stolte, J.: Calibration of the LISEM model for a small Loess Plateau catchment, CATENA, 54, 235–254, https://doi.org/10.1016/S0341-8162(03)00067-5, 2003.

Hinsberger, R., Biehler, A., and Yörük, A.: Influence of Water Depth and Slope on Roughness—Experiments and Roughness Approach for Rain-on-Grid Modeling, Water, 14, 4017, https://doi.org/10.3390/w14244017, 2022.

Jain, M. K., Kothyari, U. C., and Ranga Raju, K. G.: A GIS based distributed rainfall–runoff model, J. Hydrol., 299, 107–135, https://doi.org/10.1016/j.jhydrol.2004.04.024, 2004.

https://doi.org/10.5194/egusphere-2024-1276
Preprint. Discussion started: 30 May 2024

Järvelä, J.: Flow resistance of flexible and stiff vegetation: a flume study with natural plants, J. Hydrol., 269, 44–54, https://doi.org/10.1016/S0022-1694(02)00193-2, 2002.

Järvelä, J.: Determination of flow resistance caused by non-submerged woody vegetation, Int. J. River Basin Manag., 2, 61–70, https://doi.org/10.1080/15715124.2004.9635222, 2004.

Jarvis, N., Koestel, J., Messing, I., Moeys, J., and Lindahl, A.: Influence of soil, land use and climatic factors on the hydraulic conductivity of soil, Hydrol. Earth Syst. Sci., 17, 5185–5195, https://doi.org/10.5194/hess-17-5185-2013, 2013.

Jetten, V.: LISEM, Limburg Soil Erosion Model, User's Manual, University of Utrecht, 2002.

Kiczko, A., Västilä, K., Kozioł, A., Kubrak, J., Kubrak, E., and Krukowski, M.: Predicting discharge capacity of vegetated compound channels: uncertainty and identifiability of one-dimensional process-based models, Hydrol. Earth Syst. Sci., 24, 4135–4167, https://doi.org/10.5194/hess-24-4135-2020, 2020.

Luhar, M. and Nepf, H. M.: From the blade scale to the reach scale: A characterization of aquatic vegetative drag, Adv. Water Resour., 51, 305–316, https://doi.org/10.1016/j.advwatres.2012.02.002, 2013.

van Meerveld, H. J. (Ilja), Zhang, J., Tripoli, R., and Bruijnzeel, L. A.: Effects of Reforestation of a Degraded *Imperata* Grassland on Dominant Flow Pathways and Streamflow Responses in Leyte, the Philippines, Water Resour. Res., 55, 4128–4148, https://doi.org/10.1029/2018WR023896, 2019.

van Meerveld, H. J. (Ilja), Jones, J. P. G., Ghimire, C. P., Zwartendijk, B. W., Lahitiana, J., Ravelona, M., and Mulligan, M.: Forest regeneration can positively contribute to local hydrological ecosystem services: Implications for forest landscape restoration, J. Appl. Ecol., 58, 755–765, https://doi.org/10.1111/1365-2664.13836, 2021.

Motovilov, Y. G., Gottschalk, L., Engeland, K., and Rodhe, A.: Validation of a distributed hydrological model against spatial observations, Agric. For. Meteorol., 98–99, 257–277, https://doi.org/10.1016/S0168-1923(99)00102-1, 1999.

Nash, J. E. and Sutcliffe, J. V.: River flow forecasting through conceptual models part I — A discussion of principles, J. Hydrol., 10, 282–290, https://doi.org/10.1016/0022-1694(70)90255-6, 1970.

Nepf, H. M.: Hydrodynamics of vegetated channels, J. Hydraul. Res., 50, 262–279, https://doi.org/10.1080/00221686.2012.696559, 2012.

Nicosia, A. and Ferro, V.: Flow resistance due to shrubs and woody vegetation, Flow Meas. Instrum., 89, 102308, https://doi.org/10.1016/j.flowmeasinst.2023.102308, 2023.

Oberle, P., Kron, A., Kerlin, T., Rodriguez, E. R., and Nestmann, F.: Diskussionsbeitrag zur Fließwiderstandsparametrisierung zur Simulation von Oberflächenabflüssen infolge Starkregen, in: Dresdner Wasserbauliche Mitteilungen 65, Technische Universität Dresden, Institut für Wasserbau und technische Hydromechanik (Hg.): Wasserbau zwischen Hochwasser und Wassermangel, 129–139, 2021.

Peel, M. C.: Hydrology: catchment vegetation and runoff, Prog. Phys. Geogr. Earth Environ., 33, 837–844, https://doi.org/10.1177/0309133309350122, 2009.

Rawls, W. J., Brakensiek, D. L., and Miller, N.: Green-ampt Infiltration Parameters from Soils Data, J. Hydraul. Eng., 109, 62–70, https://doi.org/10.1061/(ASCE)0733-9429(1983)109:1(62), 1983.

Ries, F., Kirn, L., and Weiler, M.: Runoff reaction from extreme rainfall events on natural hillslopes: a data set from 132 large-scale sprinkling experiments in south-western Germany, Earth Syst. Sci. Data, 12, 245–255, https://doi.org/10.5194/essd-12-245-2020, 2020.

Ruiz Rodriguez, E.: Umgang mit Starkniederschlägen in Hessen. Auszug aus dem 3. Zwischenbericht, Hochschule RheinMain, Wiesbaden, 2017.

Saxton, K. E. and Willey, P. H.: The SPAW model for agricultural field and pond hydrologic simulation., in: Watershed models, 401–435, 2006.

Scheres, B., Schüttrumpf, H., and Felder, S.: Flow Resistance and Energy Dissipation in Supercritical Air-Water Flows Down Vegetated Chutes, Water Resour. Res., 56, e2019WR026686, https://doi.org/10.1029/2019WR026686, 2020.

Starkloff, T. and Stolte, J.: Applied comparison of the erosion risk models EROSION 3D and LISEM for a small catchment in Norway, CATENA, 118, 154–167, https://doi.org/10.1016/j.catena.2014.02.004, 2014.

https://doi.org/10.5194/egusphere-2024-1276
Preprint. Discussion started: 30 May 2024

Tobón, C. and Bruijnzeel, L. A.: Near-surface water fluxes and their controls in a sloping heterogeneously layered volcanic soil beneath a supra-wet tropical montane cloud forest (NW Costa Rica), Hydrol. Process., 35, e14426, https://doi.org/10.1002/hyp.14426, 2021.

Vargas-Luna, A., Crosato, A., and Uijttewaal, W. S. J.: Effects of vegetation on flow and sediment transport: comparative analyses and validation of predicting models: EFFECTS OF VEGETATION ON FLOW AND SEDIMENT TRANSPORT, Earth Surf. Process. Landf., 40, 157–176, https://doi.org/10.1002/esp.3633, 2015.

Wilson, C. A. M. E. and Horritt, M. S.: Measuring the flow resistance of submerged grass, Hydrol. Process., 16, 2589–2598, https://doi.org/10.1002/hyp.1049, 2002.

Wu, X., Yang, Y., He, T., Wang, Y., Liu, B., and Liu, Y.: Temporal variability of saturated hydraulic conductivity on a typical black soil slope of northeast China, CATENA, 236, 107742, https://doi.org/10.1016/j.catena.2023.107742, 2024.

Zehe, E. and Blöschl, G.: Predictability of hydrologic response at the plot and catchment scales: Role of initial conditions, Water Resour. Res., 40, 2003WR002869, https://doi.org/10.1029/2003WR002869, 2004.

Zehe, E., Graeff, T., Morgner, M., Bauer, A., and Bronstert, A.: Plot and field scale soil moisture dynamics and subsurface wetness control on runoff generation in a headwater in the Ore Mountains, Hydrol. Earth Syst. Sci., 14, 873–889, https://doi.org/10.5194/hess-14-873-2010, 2010.

Zwartendijk, B. W., van Meerveld, H. J., Ghimire, C. P., Ravelona, M., Lahitiana, J., and Bruijnzeel, L. A.: Soil water- and overland flow dynamics in a tropical catchment subject to long-term slash-and-burn agriculture, J. Hydrol., 582, 124287, https://doi.org/10.1016/j.jhydrol.2019.124287, 2020.

Zwartendijk, B. W., van Meerveld, H. J., Teuling, A. J., Ghimire, C. P., and Bruijnzeel, L. A.: Rainfall-runoff responses and hillslope moisture thresholds for an upland tropical catchment in Eastern Madagascar subject to long-term slash-and-burn practices, Hydrol. Process., 37, e14937, https://doi.org/10.1002/hyp.14937, 2023.